Spatial Pattern of Bias in Areal Rainfall Estimations and Its Impact on Hydrological Modeling: A Comparative Analysis of Estimating Areal Rainfall Based on Radar and Weather Station Networks in South Korea

Byung-Jin So
Hanyang University
Hyung-Suk Kim
Kunsan National University
Hyun-Han Kwon
hkwon@sejong.ac.kr
Sejong University

Research Article

Keywords: Areal rainfall, bias, weather station network, radar rainfall, density of weather station network

Posted Date: March 20th, 2024

DOI: https://doi.org/10.21203/rs.3.rs-3778971/v1

Additional Declarations: No competing interests reported.

Version of Record: A version of this preprint was published at Stochastic Environmental Research and Risk Assessment on April 12th, 2024. See the published version at https://doi.org/10.1007/s00477-024-02714-2.

Spatial Pattern of Bias in Areal Rainfall Estimations and Its Impact on Hydrological Modeling: A Comparative Analysis of Estimating Areal Rainfall Based on Radar and Weather Station Networks in South Korea

Byung-Jin So[a], Hyung-Suk Kim[b] and Hyun-Han Kwon[c*]

[a]Department of Civil and Environmental Engineering, Hanyang University, Ansan, Republic of Korea
[b]Department of Civil Engineering, Kunsan National University, Gunsan, Republic of Korea
[c]Department of Civil and Environmental Engineering, Sejong University, Seoul, Republic of Korea

February 13, 2024

[*]*Corresponding Author: Hyun-Han Kwon (hkwon@sejong.ac.kr)*

Abstract

Areal rainfall is routinely estimated based on the observed rainfall data using distributed point rainfall gauges. However, the data collected are sparse and cannot represent the continuous rainfall distribution (or field) over a large watershed due to the limitations of weather station networks. Recent improvements in remote-sensing-based rainfall estimation facilitate more accurate and effective hydrological modeling with a continuous spatial representation of rainfall over a watershed of interest. In this study, we conducted a systematic stepwise comparison of the areal rainfalls estimated by a synoptic weather station and radar station networks throughout South Korea. The bias in the areal rainfalls computed by the automated synoptic observing system and automatic weather system networks was analyzed on an hourly basis for the year 2021. The results showed that the bias increased significantly for hydrological analysis; more importantly, the identified bias exhibited a magnitude comparable to that of the low flow. This discrepancy could potentially mislead the overall rainfall-runoff modeling process. Moreover, the areal rainfall estimated by the radar-based approach significantly differed from that estimated by the existing Thiessen Weighting approach by 4%–100%, indicating that areal rainfalls from a limited number of weather stations are problematic for hydrologic studies. Our case study demonstrated that the gauging station density must be within 10 km^2 on average for accurate areal rainfall estimation. This study recommends the use of radar rainfall networks to reduce uncertainties in the measurement and prediction of areal rainfalls with a limited number of ground weather station networks.

Keywords: Areal rainfall, bias, weather station network, radar rainfall, density of weather station network.

Abbreviations: Automated synoptic observing system (ASOS); automatic weather system (AWS); hybrid surface rainfall (HSR); Korea Meteorological Administration (KMA); root mean square error (RMSE); receiver operating characteristic (ROC); true positive (TP); Thiessen Weighting (TW); false positive (FP).

1. Introduction

Areal rainfall, which is the average value of the rainfall distribution over a basin, is an essential factor in basin-scale hydrological analyses (Kwon et al., 2012; Kwon et al., 2020). Its accurate estimation is essential for understanding basin hydrology, managing water resources, and mitigating flood risks. Weather data are acquired through a weather station network in which one station covers an area with a radius of tens to hundreds of kilometers, poses significant challenges in accurately capturing the spatial variability of rainfall. The representative rainfall data of a basin from an irregularly distributed weather station network can be compiled by estimating the areal rainfall, which is the average rainfall of the basin. The areal rainfall can be estimated using various geostatistical approaches such as the simple arithmetic average method, Thiessen polygon method, and kriging interpolation methods by compensating for the irregular distribution of weather stations (Lima et al., 2021). These methods highlight the effort to improve the reliability of hydrological analyses, which heavily depends on the accuracy of areal rainfall estimates (Rakhecha and Singh, 2009; Teegavarapu, 2022).

Areal rainfall has been generally adopted for hydrological analysis because the spatial distribution of rainfall over a basin cannot be accurately measured with a limited number of ground stations. In general, the accuracy of areal rainfall is evaluated by analyzing the bias between estimated areal rainfalls (Chen et al., 2017; Daly et al., 1994; Hijmans et al., 2005; Kim et al., 2015; Kruizinga and Yperlaan, 1978; Li and Shao, 2010; Liu et al., 2022; Sene, 2013; So et al., 2017; Taesombat and Sriwongsitanon, 2009; Wagner et al., 2012; Xu et al., 2015; Yang et al., 2015; Zhang et al., 2016). However, existing methods have limitations in terms of model validation since model testing can be conducted only for the observed values of a weather station network. Moreover, the spatial distribution of rainfall across a watershed is not readily available, and the pattern is instead assumed to be uniform over the entire watershed. This issue is likely to intensify as the influence range for each weather station increases (Bližňák et al., 2022; Gampe and Ludwig, 2017).

Recently, recognizing the limitations of weather station networks in estimating areal rainfall, studies were conducted to explore the use of continuous rainfall data acquired from radars and satellites for determining areal rainfall. These studies investigated the performance of remote-sensing-based models for a target basin and reported that the accurate estimation of areal rainfall is strongly related to the spatial distribution of the weather station network. More importantly, the reliable calibration of hydrologic models is highly affected by the density of the weather station network, with denser networks providing an accurate representation of the rainfall-runoff process (Cheng et al., 2012; Lebel et al., 1987; Wood et al., 2000). Previous studies considered the spatio-temporal variability of continuous rainfall sequences across watersheds (Ahmed et al., 2022; Akgül and Aksu, 2021; Bližňák et al., 2022; Haberlandt, 2007; Malede et al., 2022; Schiemann et al., 2011; Sherman and Johnson, 1993; Valles et al., 2020; Verworn and Haberlandt, 2011). In addition, several studies revealed that reliable hydrological simulations could be achieved using accurate areal rainfalls from a dense weather station network considering geographical and orographic effects. However, these studies were limited to specific basins and could not be applied to other areas.

Various areal rainfall estimation methods based on weather station networks still have a clear limitation in that a direct comparison with the true rainfall field is not feasible for ungauged watersheds. Moreover, the effect of basin size on the estimation of areal rainfall averages from point rainfall estimates has been theoretically explored by previous studies (Veneziano and Langousis, 2005; Langousis and Kaleris, 2013). Veneziano and Langousis (2005) proved the scaling properties of the ARF (areal reduction factor) under the condition that spacetime rainfall has multifractal scale invariance. Moreover, they explored the bias when estimating the ARF from sparse rain gauge networks. They showed that the bias in ARF is mainly induced by estimating areal rainfalls from the rain gauge network due to the saturation of ARF, leading to 1 as basin size increases. Langousis and Kaleris (2013) developed a theoretical framework to obtain estimates of spatial rainfall averages and further used them to effectively calibrate rainfall–runoff models in basins covered by a single rain gauge. Hwang et al. (2020) assessed spatial interpolation methods for areal rainfall estimations in small South Korean catchments with limited rain gauges. It found that accuracy decreases with smaller catchment sizes and fewer gauges, particularly noting the Thiessen method's limitations. Although the study provided recommendations for optimizing the placement of rain gauges in small catchments, the potential biases associated with existing methods in rainfall-runoff modeling were not explicitly explored. Moreover, the previous study was based on data from a limited set of five radar stations. Currently, Hybrid Surface Rainfall (HSR) data sourced from 10 radar stations over South Korea, representing the latest advancement in radar synthetic rainfall data, is readily available for a more detailed assessment of how accurate spatial rainfall information impacts areal rainfall estimation. This study is not intended to directly investigate the ARF and the associated bias from sparse rain gauge networks. Instead, our focus is to better understand systematic biases in estimating areal rainfall and represent the required density of the weather station network using radar rainfall field. Here, we explore an approach for estimating accurate areal rainfall and provide a systematic procedure for the direct comparison of areal rainfalls for watersheds with a limited number of weather station networks. The accuracy and reliability of the areal rainfalls measured by a weather station network were evaluated using radar data. The main objectives of this study are threefold: first, we explored the systematic biases in estimating areal rainfall; second, the reliability of the areal rainfall based on the density of the weather station network was evaluated; and third, the optimum density of the weather station network that produces the most accurate representation of areal rainfall for a basin was determined. Finally, a strategy for estimating areal rainfall for hydrological analysis was examined.

2. Weather Station and Radar Networks

Radar data are suitable for estimating the areal rainfall of a basin because they provide high spatiotemporal resolution. Radar rainfall estimation biases arise from inaccurate radar reflectivity measurements and variability in its vertical profile, which affects the Z-R relationship. (McRoberts and Nielsen-Gammon, 2017; Seo et al., 2015; Berne and Krajewski, 2013; Hall et al., 2015). Efforts to improve accuracy include hybrid scan reflectivity precipitation estimation techniques (Fulton et al., 1998; O'Bannon, 1997; Zhang et al., 2011; Kim et al., 2018; Kim et al., 2020). For instance, the Korea Meteorological Administration (KMA) developed and provided HSR data through a multiple-elevation-based rainfall estimation approach, which involved three-dimensional data collection using a dual-polarization radar (Fulton et al., 1998; O'Bannon, 1997; Zhang et al., 2011; Nguyen et al., 2021).

In this study, three types of precipitation data enabling the examination of the spatial precipitation distribution throughout South Korea were selected. These include automated synoptic observing system (ASOS) data from 96 stations, automatic weather system (AWS) data from 504 stations, and HSR data which are synthesized radar data from 10 stations. All of them are simultaneously operated such that a dense network of precipitation data across South Korea can be acquired on an hourly basis. This study used hourly precipitation data from the three types of weather stations for the year 2021, as shown in Figure 1 and Table 1. All the data were transformed into a one-hour temporal scale to obtain the spatial distribution of hourly precipitation over an entire watershed. KMA provides weather and climate data through its open meteorological data portal (https://data.kma.go.kr).

[Insert Figure 1 and Table 1]

Hydrologic unit maps delineate watersheds in terms of size (large, middle, and standard) with watershed characteristics. These maps are used for collecting and analyzing the data for managing water resources. These maps are shared between organizations at the local and national level to improve water use efficiency, planning, and management. In general, hydrological analysis is carried out on a watershed basis, and the areal rainfall representing the average rainfall over the target watershed is estimated first. In Korea, hydrologic unit maps are managed and updated by the Ministry of Environment (MOE). A hydrologic unit map is composed of 20 large basins (LBSN), 106 middle sized basins (MBSN), and 808 standard basins (SBSN), as shown in Figure 2 and Table 2.

[Insert Figure 2 and Table 2]

3. Research Methods and Evaluation Metrics

Basin-scale hydrological analysis requires the average rainfall over the entire watershed. Traditional methods such as the Thiessen Weighting (TW) and inverse distance weighting (IDW) have been used to estimate areal rainfall using sparse ground station data. In this study, we focus on the role of spatial continuity for estimating the areal rainfall and the limitation of existing approaches in accurately determining the areal rainfall. It should be noted that bias in the precipitation amounts obtained from radar rainfall estimates is not explicitly explored, and this study investigates the enhancement of ground weather station networks with spatial information from radar rainfall field data. This study follows a three-step process. In the first step, existing areal rainfall estimation approaches are systematically compared. Specifically, the areal rainfall measurements from ASOS and AWS are compared for a given hydrologic unit. The measurement differences are investigated in terms of amounts and spatial patterns. In the second step, the performance of radar in estimating areal rainfall is evaluated by replacing the observed precipitation obtained from ASOS or AWS weather stations with the radar rainfall estimates for the same locations. Although the radar rainfall field is not expected to be identical to the observed data of the weather station, areal rainfalls based on radar rainfall estimates can be used to explore the role of the density of the weather station network. Moreover, the estimated areal rainfalls in this stage are subsequently used to compare true areal rainfalls based on entire radar rainfall estimates over the basin for a consistent comparison. In the third step, two types of areal rainfall data, obtained from pointwise radar rainfall estimates at the same locations of the weather station networks (i.e., ASOS and AWS) and gridded radar rainfall estimates averaged over the basin, are compared. Here, the areal rainfalls estimated from the entire grid are used to better understand the limitations and advantages of estimating the areal rainfall of a basin according to the density of weather stations in a hydrologic unit. The accurate representation of the areal rainfall could be achieved through this three-step process. Through this process, the areal rainfall in terms of the weather station network density and the watershed area is comprehensively analyzed, and the optimal spatial density of a weather station network for the effective estimation of the areal rainfall for basin-scale hydrological analysis is investigated. Figure 3 presents the detailed modeling process employed in our comparative analysis.

[Insert Figure 3]

In this study, the TW method is applied to estimate the area-weighted areal rainfall of a watershed from weather stations and radar networks. Three types are described by the following equations.

Type 1: Areal rainfall by the TW method on weather network data ($P_{a,wsn}$) is expressed as

$$P_{a,wsn} = \frac{\sum_i^N (P_{i,wsn} \times Area_i)}{Area_{watershed}} \qquad (1)$$

where N is the number of weather stations in the watershed and $P_{i,wsn}$ is the precipitation from the weather station network observed at station i.

Type 2: Areal rainfall by the TW method which involves replacing the rainfall amounts with the radar rainfall estimates ($P'_{a,wsn}$) at the nearest grids to point gauges at the location weather network is expressed as

$$P'_{a,wsn} = \frac{\sum_i^N (P_{i,rwsn} \times Area_i)}{Area_{watershed}}, \tag{2}$$

where N is the number of weather stations in the watershed and $P_{i,rwsn}$ is the radar rainfall estimates for the weather station network at station i.

Type 3: Areal rainfall by the mean radar rainfall ($P_{a,rn}$) that is assumed to be the true areal rainfall is calculated as

$$P_{a,rn} = \frac{\sum_j^N (P_{j,rn} \times Drained\_Area_j)}{Area_{watershed}}, \tag{3}$$

where N is the number of grids in the watershed and $P_{j,rn}$ is the precipitation from the radar network observed at grid j.

In addition, three different goodness-of-fit (GoF) metrics (Ralph, 1986) are used to evaluate the similarity of rainfall patterns and areal rainfall. These GoF metrics are the root mean square error (RMSE), correlation coefficients (CC) and receiver operating characteristic (ROC) curve, and correlation coefficient between the areal rainfalls. The GoF metrics are calculated as follows:

$$RMSE = \sqrt{\frac{\sum_i^T \left(P_{a,wsn}^i - P_{a,rn}^i\right)^2}{N}}, \tag{4}$$

where $P_{a,wsn}^i$ and $P_{a,rn}^i$ represent the areal rainfall estimated by the TW method based on weather network data and by averaging radar rainfall data at the i^{th} time step, respectively, while T denotes the length of the time series.

$$CC = \mathrm{r}_{xy} = \frac{\sum_i^T \left(P^i_{a,wsn} - \overline{P_{a,wsn}}\right)\left(P^i_{a,rn} - \overline{P_{a,rn}}\right)}{\sqrt{\sum_i^T \left(P^i_{a,wsn} - \overline{P_{a,wsn}}\right)^2 \sum_j^N \left(P^i_{a,rn} - \overline{P_{a,rn}}\right)^2}}, \tag{5}$$

where r_{xy} is the correlation coefficients and *T* is the length of the areal rainfall time series

Consider a two-class prediction problem (binary classification) in which the outcomes are classified as either positive (*p*) or negative (*n*). The number of possible outcomes from a binary classifier is four. If the outcome from a prediction is *p* and the actual value is also *p*, then the result is called a true positive (TP). If the actual value is *n*, then the result is called a false positive (FP). Conversely, a true negative (TN) occurs when both the prediction outcome and the actual value are *n*, and a false negative (FN) occurs when the prediction outcome is *n* while the actual value is *p*. Here, the true positive rate (TPR) and the false positive rate (FPR) are needed (as functions of some classifier parameter) to derive a ROC curve (Peterson et al., 1954; Wilks, 2006). Specifically, the ROC curve is the plot of the TPR against the FPR at various threshold settings. The area under the ROC curve (AUC) serves as a comprehensive metric for assessing the accuracy of forecasts, commonly referred to as the ROC score. AUC allows for an objective comparison between models. In the ideal scenario, where forecasts are perfect, the ROC curve will converge to a point at (FPR=0, TPR=1.0), indicating an AUC of 1.0—the maximum achievable score. Conversely, forecasts exhibiting little to no predictive skill will achieve a score close to an AUC of 0.5, corresponding to the area under a diagonal line that represents random-guess level performance. One of the key advantages of using AUC as a metric is its independence from any specific classification threshold. This makes it particularly useful for evaluating and comparing models when the optimal threshold is not known or may vary depending on different operational or business requirements. The TPR defines how many correct positive results occur among all positive samples available during the testing period. The FPR defines how many incorrect positive results occur among all negative samples available during the testing period. Therefore, the

FPR and TPR are used to define a ROC space in the x and y axes, respectively. For example, the best case for the predictive value would yield a point in the upper left corner or coordinate (0, 1) of the ROC space, representing 100% sensitivity (no FNs) and 100% specificity (no FPs).

$$\mathrm{TPR} = \frac{\mathrm{TP}}{P} = \frac{TP}{TP+FN} \tag{6}$$

$$\mathrm{FPR} = \frac{\mathrm{FP}}{N} = \frac{FP}{FP+TN} \tag{7}$$

This study generated the ROC curves for the estimated areal rainfalls collected by the ASOS and AWS weather station networks. The consistency of the rainfall patterns between the two areal rainfall sequences for the same watershed was evaluated by assigning 1 for rainfall detection and 0 for no rainfall detection for given rainfall occurrences in the areal rainfall time series.

[Insert Figure 4]

4. Results

4.1 Reliability assessment for areal rainfall using the TW method

Two types of weather station networks (ASOS and AWS) are operated across the South Korea. The TW method was used to estimate the areal rainfall for hydrologic units based on data from each type of weather observation network. The estimated areal rainfalls from the two types of weather station networks were compared. Here, areal rainfalls are solely based on the observed precipitation obtained from weather station networks to better understand the role of the spatial distribution of rainfall gauges in accurately estimating areal rainfalls. By analyzing the ROC curves of the ASOS- and AWS-based areal rainfalls for all basins, the spatial patterns of the two areal rainfalls were compared to identify similarities and dissimilarities. Comparisons were made with the complete rainfall sequences, including zero rainfall. The ROC score is directly estimated by comparing spatial rainfall patterns obtained from ASOS- and AWS weather station networks. The AWS weather station network is composed of more than 500 stations, while there are 96 stations for the ASOS weather station network. Thus, one can expect that the AWS-based areal rainfall measurements can depict spatial patterns of rainfall fields more accurately. Meanwhile, the ASOS-based area rainfall estimation can be ineffective for smaller basins such as SBSNs (Hyun et al., 2019); hence, the dissimilarities in the ROC scores are expected to be higher for the smaller basins than for the middle and large basins. The results showed that the ROC score lies in the range of 0.8–0.98 for SBSNs, 0.84–0.96 for MBSNs, and 0.89–0.97 for LBSNs. As expected, the similarity of rainfall patterns between the two areal rainfalls increases with the watershed area. The ROC scores for SBSNs had a much larger range compared to those for the LBSNs, as seen in Figure 5.

[Insert Figure 5]

The RMSE was calculated to quantitatively evaluate biases (or differences) in areal amounts derived from the ASOS and AWS weather station networks over South Korea. The spatial pattern of the RMSE and their distributions with different basin sizes are illustrated in Figures 6 and 7, respectively. The RMSE (mm/h) was found to be 0.02–0.12 for SBSNs, 0.03–0.09 for MBSNs, and 0.015–0.06 for LBSNs. As expected, the similarity of rainfall patterns between the two areal rainfalls increases with the watershed area, and the RMSEs of SBSNs showed a much larger range compared to those of the LBSNs, as seen in Figure 7.

[Insert Figures 6 and 7]

We estimated the RMSE for the rainfall events, excluding the zero rainfalls, in the same manner as illustrated in Figures 6 and 7. As shown in Figures 8 and 9, the RMSE (mm/h) range was 0.2–1.12 for SBSNs, 0.22–0.7 for MBSNs, and 0.08–0.45 for LBSNs. The RMSE for the nonzero rainfall series stood out as being more prominent and increased by six to ten times compared to the RMSE for the complete time series, which included zero rainfalls. The spatial pattern of the RMSE (Figure 8) over South Korea was similar to that of the complete series, while an increasing tendency was also clearly observed in the distribution of the RMSE with different basin sizes, as displayed in Figure 9.

[Insert Figures 8 and 9]

The Soyang River basin was selected for further research into these biases as crucial for improving areal rainfall estimates with limited rain gauges. The basin holds significant importance in the management of water resources within South Korea, supported by the presence of highly reliable, long-term rainfall, and runoff data. Figure 10 showed the observed runoff series measured from the Soyang River basin (2,783.26 km^2), one of the MBSNs, together with the average RMSE in m^3/s. There are approximately 90 days with measurements below the black line, indicating a low water flow condition. More specifically, the RMSE was comparable in magnitude to that of the low flow condition, potentially misleading the overall rainfall-runoff modeling process. The bias in the estimation process of areal rainfalls should be reduced by considering the accurate spatial pattern of rainfall informed by radar networks.

[Insert Figure 10]

4.2 Understanding biases in the estimation of areal rainfalls

The reliability of areal rainfall measurements is mainly affected by the density of the ASOS and AWS networks, and we demonstrated a high gauge density is needed to accurately represent areal rainfalls. A systematic experiment with three different strategies was designed to explore the accuracy of areal rainfall estimation in terms of the density of gauging stations. Areal rainfalls are estimated with the radar rainfall networks based on the locations of ASOS and AWS weather stations. More specifically, the radar-based rainfall measurements for the locations of ASOS and AWS stations were first extracted, and the TW method was applied for constructing areal rainfalls. Cross-correlations of the precipitation series over the ASOS and AWS stations were illustrated in Figures 11(a) and 11(b). The cross-correlations of radar rainfall estimates obtained for the same locations as the ASOS and AWS weather station networks were compared in Figures 11(c) and 11(d). As seen in Figure 10, radar rainfall estimates accurately reproduce spatial dependency across stations obtained from the ASOS and AWS stations. Therefore, areal rainfalls averaged over entire radar-gridded networks encompassing target basins are assumed to be the true areal rainfall. Here, bias in radar rainfall estimates is not considered for the estimation of areal rainfalls, and this study instead focuses on exploiting spatial patterns of radar-measured rainfall. Further, one can expect consistent comparisons across three different cases in estimating areal rainfalls.

[Insert Figure 11]

Figure 12 revealed the difficulties in correctly estimating areal rainfalls with actual rainfall fields and the limited number of ground gauges based on the TW method. In the figure, a rainfall distribution exists in the basin, but the areal rainfall in the basin can be zero if rainfall is not detected by the weather observation network. In contrast, the areal rainfall can be overestimated if the rainfall distribution is only observed in the limited part of the area with a larger weighing factor *(Kim et al., 2018; Hwang et al., 2020)*. In this context, biases could be expanded with extreme weather events (*Nguyen et al., 2021; So et al., 2015*).

[Insert Figure 12]

We further investigated biases in the weighting factor of the TW method by repeatedly estimating areas covered by actual rainfall fields over time with respect to the Thiessen polygons in the Soyang River basin (i.e., a MBSN). Figure 13 shows the radar-based TW weighting factor sequences for six contributing areas with the representative gauging stations in the Soyang River basin, while the red line is the existing TW weighting factor used to estimate areal rainfalls. The radar-based TW weighting factor sequences showed a noticeable change over time in the range of 4%–100% with respect to the existing TW weighting factor. More importantly, during the non-rainy season, spanning from November to April, the weighting factors were noticeably distributed from zero to the maximum value, representing the existing TW factor. Conversely, during the rainy season from May to early October, there was significant variability covering the entire range of the weighting factor as illustrated in representative stations No. 90, 93, 100, 101, and 211. However, station No. 212 showed no discernible change over the entire year due to its relatively low contributing area (TW factor of 0.0005) for the Soyang River basin. This indicates that the areal rainfalls based on the weighting factor from a limited number of gauging stations could be problematic in effectively representing spatial rainfall patterns, leading to inaccurate estimation of areal rainfall.

[Insert Figure 13]

The weighing factors informed by the ASOS (low density) and AWS (high density) networks were then applied to examine the effectiveness of a higher density of weather stations in estimating areal rainfalls, as illustrated in Figure 14. The areal rainfall obtained from radar rainfall estimates on ASOS showed significant biases compared to the true areal rainfall (labeled Radar) averaged over gridded radar rainfalls. At the same time, a noticeable improvement was identified with the radar rainfall estimates on AWS. For the case of the ASOS station, the overestimation mainly occurs with large rainfall amounts, whereas the underestimation occurs with small rainfall amounts. The consistency of the rainfall patterns between the two areal rainfall time series for the same basin was further evaluated by substituting 1 for rainfall and 0 for no rainfall according to the rainfall occurrence in the areal rainfall time series. It was found that the mismatch ratios were about 10.9% and 5.3% for the

ASOS and AWS networks, respectively. Further, the ROC score is illustrated in Figure 15. The ROC score between the ASOS-based (or AWS-based) areal rainfalls and true areal rainfalls lies in the range of 0.84–0.97 (or 0.92-0.98) for SBSNs, 0.86–0.96 (or 0.94-0.98) for MBSNs, and 0.91–0.96 (0.96-0.98) for LBSNs. It can be concluded that the consistency of rainfall patterns between the ASOS-based (or AWS-based) areal rainfalls and true areal rainfalls increases with the density of the weather station network. Moreover, the ROC score in SBSNs represents increased variability (or range) while a much tighter band is observed for LBSNs.

[Insert Figures 14 and 15]

This study compared the correlation coefficients (Figure 16) and the RMSEs (Figures 17 and 18) to better characterize the similarity between areal rainfall series. It was found that the correlation coefficient increases and the RMSE decreases as the weather station network density and the watershed area are increased, indicating that the areal rainfall informed by a high density of weather station network (i.e., the AWS network) becomes similar to the true spatial rainfall pattern. The RMSE for the rainfall time series, excluding the zero rainfalls (Figure 18), turns out to be more significant and higher by tenfold than the RMSE for the complete areal rainfall series, including the zero rainfalls (Figure 17). Thus, the systematic bias in estimating areal rainfalls with respect to the weather station network needs to be corrected by an increase in the density of the weather station network, leading to the accurate spatial pattern representation of rainfall.

[Insert Figures 16, 17 and 18]

Finally, the contributing area ratio, defined as the ratio of the contributing area covered by the actual rainfall field to the Thiessen polygons, was evaluated for all basins and all rainfall series, as illustrated in Figure 19. A value of 100 indicates that the contributing rainfall area on the Thiessen polygons is the same as the existing TW weight factor, and a value closer to zero represents that the actual rainfall field with respect to the Thiessen polygons is relatively smaller. As shown in Figure 19, the results support a clear inverse relationship between the Thiessen polygon area and the ratio. The variability (or range) of the contributing ratio becomes larger with a relatively small Thiessen polygon area, indicating that rainfall variability is higher in for areas smaller than approximately 10 km^2. In contrast, as the polygon area is increased, the variability is gradually decreased. For example, to reduce the difference in the ratio by 10%, the density of the weather station network needs to be within 10 km^2 in the average sense, although the variability will be relatively higher.

5. Discussion

This study provided a detailed comparison of areal rainfall estimates derived from two types of weather station networks (ASOS and AWS) across various hydrologic units in South Korea. Unlike many previous studies, which may focus on a specific basin size, our analysis spans small to large basins (SBSNs, MBSNs, and LBSNs), offering a broader perspective on the spatial accuracy of rainfall estimation. Consistent with Hyun et al. (2019), this study demonstrated that the AWS network, with a higher density of weather stations, shows more accurate spatial patterns of rainfall, especially in smaller basins (SBSN), compared to the ASOS network. This emphasizes the critical role of weather station density in capturing the spatial variability of rainfall across different hydrologic units, a similar concept highlighted in various studies in the field of hydrologic science (Kim et al., 2018; Hwang et al., 2020). In contrast to the findings of Nguyen et al. (2021) and So et al. (2015), which suggest that bias associated with extreme weather events may be exacerbated in networks with sparse station density, our analysis extended this understanding by quantifying the extent of bias across various basin sizes and rainfall intensities.

In this study, several methodological advancements over previous research were introduced. Firstly, we offered a detailed analysis of how the density of weather station networks affects the accuracy of areal rainfall estimates. This was achieved by using a different set of Goodness-of-Fit (GoF) metrics, encompassing both the ROC score and RMSE value across a range of basin sizes and rainfall intensities. Secondly, the integration of radar rainfall estimates into our study provided a systematic comparative framework for evaluating the performance of ground-based observations in estimating areal rainfall. This comparative analysis, which is relatively limited in the existing research, enhanced our understanding by highlighting the capabilities and limitations of ground-based observations compared to radar rainfall estimates. Thirdly, we investigated how biases identified in areal rainfall estimates can impact runoff predictions in the Soyang River basin. Our findings on the discrepancies between areal rainfall estimates from ASOS and AWS networks have direct implications for rainfall-runoff modeling in the Soyang River basin. The RMSE values, especially when comparing biases associated with areal rainfall estimates to observed runoff, emphasized the sensitivity of runoff predictions to the accuracy of rainfall inputs. This was exemplified by the comparable magnitude of RMSEs to low flow conditions observed in the basin, suggesting that inaccuracies in rainfall estimation could lead to substantial biases in modeling the rainfall-runoff process, especially during periods of low flow.

The potential biases in radar rainfall estimates, which were not accounted for in our analysis, could influence the accuracy of areal rainfall estimations. Furthermore, the generalization of our results may be constrained by regional climatic and topographical characteristics within South Korea. Future research should aim to address these biases and explore the applicability of our findings in different hydrological and climatic contexts. Additionally, exploring the impact of quasi-real-time data integration and advancements in radar technology on areal rainfall estimation accuracy could provide valuable insights for the hydrological community.

Our study emphasized the significance of optimizing weather station network density for improving areal rainfall estimates, which are crucial for hydrological modeling, flood forecasting, and water resource management. Accurate areal rainfall estimation can significantly enhance the reliability of rainfall-runoff models, contributing to more effective water resource planning and management strategies. The variability in estimation accuracy across different basin sizes and network densities highlights the need for tailored approaches in deploying weather station networks, especially in regions prone to extreme weather events. Thus, it should be noted that a sensitivity analysis on the variability of the contributing ratio could significantly enhance our understanding of the dynamics between weather station density, the accuracy of areal rainfall estimation, and the performance of hydrological models. In this context, future efforts will concentrate on understanding the impact of weather station density on the accuracy of areal rainfall estimation, especially concerning the critical threshold of the weather station density. This analysis aims to explore optimal strategies for deploying weather stations, offering valuable insights for water resource management and fostering more resilient and adaptive hydrological practices in response to climatic variability.

[Insert Figure 19]

6. Conclusions

In this study, we explored the systematic bias in estimating the areal rainfall for a basin in the context of the density of the weather station network. For this purpose, radar rainfall estimates were utilized to better understand the required density of the weather station network for accurate areal rainfall estimation. Further, we compared areal rainfall estimates for different basin sizes using a limited number of weather station networks. A stepwise procedure was developed to systematically evaluate areal rainfalls with an existing ground weather station and radar station networks. The main findings and recommendations of this study are as follows.

1. The areal rainfalls estimated by the ASOS and AWS weather station networks for different hydrologic units were compared, and the discrepancies in the estimated areal rainfalls were evaluated. Here, areal rainfalls were solely derived from the observed precipitation over the weather station network to characterize the role of the spatial distribution of rainfall gauges. We calculated the ROC scores and compared spatial rainfall patterns from ASOS and AWS weather station networks. As expected, the AWS-based areal rainfalls obtained from more than 500 stations were more effective than the ASOS-based areal rainfalls from 96 stations in terms of representing the spatial patterns of rainfall fields. The variation in the ROC scores was higher for the smaller basins than for the larger basins. Alternatively, the similarity of rainfall patterns between the two areal rainfalls increased with the watershed area. The ROC scores for the smaller basins (SBSNs) demonstrated more variability, while those for the larger basins (LBSNs) were higher.

2. The bias in the areal rainfall was explored by determining the RMSE between the areal rainfalls estimated from the ASOS and AWS weather station networks. The RMSE was found to be significant, especially for modeling the hydrological process. More importantly, the RMSE was comparable in magnitude to that of the low flow condition and was relatively high with respect to the observed flow rate, misleading the overall rainfall-runoff modeling process. Therefore, reduction of bias in the areal rainfalls is required for an accurate representation of the rainfall-runoff modeling process. This study recommends the use of spatial patterns of rainfall informed by radar rainfall networks to reduce the bias of the areal rainfalls estimated by a limited number of ground weather station networks.

3. Radar-based rainfall measurements for the locations of the ASOS and AWS stations were extracted and compared with the areal rainfalls averaged from grids over the target basin that were assumed to be the true values. As a case study, biases in the weighting factor of the TW method were evaluated by estimating areas covered by radar rainfall fields over time with respect to the Thiessen polygons over the Soyang River basin. It was found that the radar-based TW weighting factors were significantly different from that of the existing TW in the range of 4%–100%, demonstrating that the areal rainfalls from a limited number of stations are problematic for hydrologic studies. The areal rainfall estimated from radar rainfall estimates on ASOS showed a noticeable increase in bias compared with the radar rainfall estimates on AWS with respect to the true areal rainfall averaged over gridded radar rainfalls. For lower density weather station networks, higher rainfall intensity was overestimated, whereas low rainfall intensity was underestimated. Similarly, the ROC score between the AWS-based areal rainfalls and true areal rainfalls showed an improved agreement. The results confirmed that the consistency between estimated areal rainfalls and true areal rainfalls increases with the density of the weather station network, and its effect was more prominent for large basins.

4. The contributing area ratio, defined by the actual rainfall areas with respect to the Thiessen polygons, showed a clear inverse relationship with the Thiessen polygon area, whereas the associated variability is enlarged with a relatively small area and vice versa for the larger polygon area. If one intends to minimize the bias in the estimation of areal rainfall within approximately 10%, our case study demonstrated that the gauging station density needs to be within 10 km^2 in the average sense.

This study recommends utilizing a radar station network for understanding the bias in the areal rainfall estimation and examining the required density of weather stations for accurate hydrological modeling, especially for larger basins. The future research will combine rainfall-runoff modeling with the areal rainfall estimation process to reduce uncertainty in hydrological analysis over different basin sizes and rainfall patterns.

Acknowledgement

This work was supported by Korea Environment Industry & Technology Institute (KEITI) through Water Management Program for Drought, funded by Korea Ministry of Environment (MOE) (2022003610003). We thank the associate editor and two anonymous reviewers for the valuable comments that greatly improved the original version of the manuscript.

Declarations

Ethical Approval Not applicable.

Consent to Participate Not applicable.

Consent to Publish Not applicable.

Authors Contributions Byung-Jin So: conceptualization, data curation, methodology, software, validation, formal analysis, writing - original draft preparation. **Hyung-Suk Kim**: supervision, writing - review & editing. **Hyun-Han Kwon**: conceptualization, methodology, validation, investigation, supervision, writing - review & editing, funding acquisition

Funding This work was supported by Korea Environment Industry & Technology Institute (KEITI) through Water Management Program for Drought, funded by Korea Ministry of Environment (MOE) (2022003610003).

Competing Interests The authors declare that they have no conflict of interest.

Availability of data and materials Precipitation data and Composite Radar HSR are freely available from https://data.kma.go.kr.

Reference

Ahmed, S.I., Sharma, R., Goel, P., Khan, A., Gharabaghi, B., Rudra, R., 2022. A comparative evaluation of using rain gauge and NEXRAD radar-estimated rainfall data for simulating streamflow. Hydrology 9(8), 133. https://doi.org/10.3390/hydrology9080133

Akgül, M.A., Aksu, H., 2021. Areal precipitation estimation using satellite derived rainfall data over an irrigation area. Turkish Journal of Agriculture - Food Science and Technology 9(2), 386–394. https://doi.org/10.24925/turjaf.v9i2.386-394.4061

Berne, A., Krajewski, W.F., 2013. Radar for hydrology: Unfulfilled promise or unrecognized potential? Adv Water Resour 51. https://doi.org/10.1016/j.advwatres.2012.05.005

Bližňák, V., Pokorná, L., Rulfová, Z., 2022. Assessment of the capability of modern reanalyses to simulate precipitation in warm months using adjusted radar precipitation. J Hydrol Reg Stud 42, 101121. https://doi.org/10.1016/J.EJRH.2022.101121

Chen, T., Ren, L., Yuan, F., Yang, X., Jiang, S., Tang, T., Liu, Y., Zhao, C., Zhang, L., 2017. Comparison of spatial interpolation schemes for rainfall data and application in hydrological modeling. Water (Switzerland) 9(5), 342. https://doi.org/10.3390/w9050342

Cheng, C.D., Cheng, S.J., Wen, J.C., Lee, J.H., 2012. Effects of raingauge distribution on estimation accuracy of areal rainfall. Water Resour Manag 26(1), 1–20. https://doi.org/10.1007/s11269-011-9898-7

Daly, C., Neilson, R.P., Phillips, D.L., 1994. A statistical-topographic model for mapping climatological precipitation over mountainous terrain. J Appl Meteorol 33(2), 140–158. https://doi.org/10.1175/1520-0450(1994)033<0140:ASTMFM>2.0.CO;2

Fulton, R.A., Breidenbach, J.P., Seo, D.J., Miller, D.A., O'Bannon, T., 1998. The WSR-88D rainfall algorithm. Weather Forecast 13(2), 377–395. https://doi.org/10.1175/1520-0434(1998)013<0377:TWRA>2.0.CO;2

Gampe, D., Ludwig, R., 2017. Evaluation of gridded precipitation data products for hydrological applications in complex topography. Hydrology 4(4), 53. https://doi.org/10.3390/hydrology4040053

Haberlandt, U., 2007. Geostatistical interpolation of hourly precipitation from rain gauges and radar for a large-scale extreme rainfall event. J Hydrol (Amst) 332(1–2), 144–157. https://doi.org/10.1016/j.jhydrol.2006.06.028

Hall, W., Rico-Ramirez, M.A., Krämer, S., 2015. Classification and correction of the bright band using an operational C-band polarimetric radar. J Hydrol (Amst) 531, 248–258. https://doi.org/10.1016/j.jhydrol.2015.06.011

Hijmans, R.J., Cameron, S.E., Parra, J.L., Jones, P.G., Jarvis, A., 2005. Very high resolution interpolated climate surfaces for global land areas. Int J Climatol 25(15), 1965–1978. https://doi.org/10.1002/joc.1276

Hwang, S. H., Kim, K. B. and Han, D., 2020. Comparison of methods to estimate areal means of short duration rainfalls in small catchments, using rain gauge and radar data. Journal of Hydrology, 588, 125084.

Hyun, J.H., Park, H. and Chung, G., 2019. Effects of the Difference between ASOS and AWS Data on Runoff Characteristics. Journal of The Korean Society of Hazard Mitigation, 19(7), pp.443-449.

Kim, K.B., Kwon, H.H. and Han, D., 2015. Bias correction methods for regional climate model simulations considering the distributional parametric uncertainty underlying the observations. *Journal of Hydrology*, 530, pp.568-579.

Kim, T.J., Kwon, H.H. and Lima, C., 2018. A Bayesian partial pooling approach to mean field bias correction of weather radar rainfall estimates: Application to Osungsan weather radar in South Korea. Journal of Hydrology, 565, pp.14-26.

Kim, T.J., Kwon, H.H. and Kim, K.B., 2021. Calibration of the reflectivity-rainfall rate (ZR) relationship using long-term radar reflectivity factor over the entire South Korea region in a Bayesian perspective. Journal of Hydrology, 593, p.125790.

Kruizinga, S., Yperlaan, G.J., 1978. Spatial interpolation of daily totals of rainfall. J Hydrol (Amst) 36(1–2), 65–73. https://doi.org/10.1016/0022-1694(78)90037-9

Kwon, H.H., de Assis de Souza Filho, F., Block, P., Sun, L., Lall, U. and Reis Jr, D.S., 2012. Uncertainty assessment of hydrologic and climate forecast models in Northeastern Brazil. *Hydrological Processes*, 26(25), pp.3875-3885.

Kwon, M., Kwon, H.H. and Han, D., 2020. A hybrid approach combining conceptual hydrological models, support vector machines and remote sensing data for rainfall-runoff modeling. *Remote Sensing*, 12(11), p.1801.

Langousis, A. and Kaleris, V., 2013. Theoretical framework to estimate spatial rainfall averages conditional on river discharges and point rainfall measurements from a single location: an application to western Greece. Hydrology and Earth System Sciences, 17(3), pp.1241-1263.

Lebel, T., Bastin, G., Obled, C., Creutin, J.D., 1987. On the accuracy of areal rainfall estimation: a case study. Water Resour Res 23(11), 2123–2134. https://doi.org/10.1029/WR023i011p02123

Li, M., Shao, Q., 2010. An improved statistical approach to merge satellite rainfall estimates and raingauge data. J Hydrol (Amst) 385(1–4), 51–64. https://doi.org/10.1016/j.jhydrol.2010.01.023

Lima, C.H., Kwon, H.H. and Kim, Y.T., 2021. A Bayesian Kriging model applied for spatial downscaling of daily rainfall from GCMs. *Journal of Hydrology*, 597, p.126095.

Liu, Y., Zhuo, L., Pregnolato, M., Han, D., 2022. An assessment of statistical interpolation methods suited for gridded rainfall datasets. Int J Climatol 42(5), 2754–2772. https://doi.org/10.1002/joc.7389

Malede, D.A., Agumassie, T.A., Kosgei, J.R., Pham, Q.B., Andualem, T.G., 2022. Evaluation of satellite rainfall estimates in a rugged topographical basin over South Gojjam Basin, Ethiopia. J Indian Soc Remote Sens 50, 1333–1346. https://doi.org/10.1007/s12524-022-01530-x

McRoberts, D.B., Nielsen-Gammon, J.W., 2017. Detecting beam blockage in radar-based precipitation estimates. J Atmos Ocean Technol 34(7), 1407–1422. https://doi.org/10.1175/JTECH-D-16-0174.1

Nguyen, D.H., Kim, S.H., Kwon, H.H. and Bae, D.H., 2021. Uncertainty Quantification of Water Level Predictions from Radar-based Areal Rainfall Using an Adaptive MCMC Algorithm. Water Resources Management, 35(7), pp.2197-2213.

O'Bannon, T., 1997. Using a `terrain-based' hybrid scan to improve WSR-88D precipitation estimates. In *Preprints, 28th Conf. on Radar Meteorology, Austin, TX, Amer Meteor Soc* Vol. 506, p. 507.

Peterson W., Birdsall T., Fox W., 1954. The theory of signal detectability. IEEE Transactions on Information Theory 4(4), 171–212. https://doi.org/ 10.1109/TIT.1954.1057460.

Rakhecha, P.R., Singh, V.P., 2009. Applied Hydrometeorology. Springer Dordrecht. https://doi.org/10.1007/978-1-4020-9844-4

Ralph B. D`Agostino., 1986. Goodness-of-Fit-Techniques. Marcel Dekker, INC. ISBN 9780367580346.

Schiemann, R., Erdin, R., Willi, M., Frei, C., Berenguer, M., Sempere-Torres, D., 2011. Geostatistical radar-raingauge combination with nonparametric correlograms: methodological considerations and application in Switzerland. Hydrol Earth Syst Sci 15(5), 1515–1536. https://doi.org/10.5194/hess-15-1515-2011

Sene, K., 2013. Flash Floods: Forecasting and Warning. Springer Dordrecht. https://doi.org/10.1007/978-94-007-5164-4

Seo, B.C., Krajewski, W.F., Mishra, K.V., 2015. Using the new dual-polarimetric capability of WSR-88D to eliminate anomalous propagation and wind turbine effects in radar-rainfall. Atmos Res 153, 296–309. https://doi.org/10.1016/j.atmosres.2014.09.004

Sherman, U.D., Johnson, L.E., 1993. Mean areal precipitation estimation using radar. In *Proceedings of the Symposium on Engineering Hydrology*, pp. 638–688.

So, B.J., Kwon, H.H., Kim, D. and Lee, S.O., 2015. Modeling of daily rainfall sequence and extremes based on a semiparametric Pareto tail approach at multiple locations. *Journal of Hydrology*, 529, pp.1442-1450.

So, B.J., Kim, J.Y., Kwon, H.H. and Lima, C.H., 2017. Stochastic extreme downscaling model for an assessment of changes in rainfall intensity-duration-frequency curves over South Korea using multiple regional climate models. *Journal of Hydrology*, 553, pp.321-337.

Taesombat, W., Sriwongsitanon, N., 2009. Areal rainfall estimation using spatial interpolation techniques. ScienceAsia 35(3), 268–275. https://doi.org/10.2306/scienceasia1513-1874.2009.35.268

Teegavarapu, R.S.V., 2022. Mean areal precipitation estimation: methods and issues. In *Rainfall: Modeling, Measurement and Applications*, pp. 217–260. https://doi.org/10.1016/B978-0-12-822544-8.00001-9

Valles, J., Corzo, G., Solomatine, D., 2020. Impact of the mean areal rainfall calculation on a modular rainfall-runoff model. J Mar Sci Eng 8(12), 980. https://doi.org/10.3390/jmse8120980

Veneziano, D. and Langousis, A., 2005. The areal reduction factor: A multifractal analysis. Water Resources Research, 41(7).

Verworn, A., Haberlandt, U., 2011. Spatial interpolation of hourly rainfall-effect of additional information, variogram inference and storm properties. Hydrol Earth Syst Sci 15(2), 569–584. https://doi.org/10.5194/hess-15-569-2011

Wagner, P.D., Fiener, P., Wilken, F., Kumar, S., Schneider, K., 2012. Comparison and evaluation of spatial interpolation schemes for daily rainfall in data scarce regions. J Hydrol (Amst) 464, 388–400. https://doi.org/10.1016/j.jhydrol.2012.07.026

Wilks, D.S. 2006. Statistical Methods in the Atmospheric Sciences. Academic Press: Cambridge, MA, USA. Volume 91, p. 627.

Wood, S.J., Jones, D.A., Moore, R.J., 2000. Accuracy of rainfall measurement for scales or hydrological interest. Hydrol Earth Syst Sci 4(4), 531–543. https://doi.org/10.5194/hess-4-531-2000

Xu, W., Zou, Y., Zhang, G., Linderman, M., 2015. A comparison among spatial interpolation techniques for daily rainfall data in Sichuan Province, China. Int J Climatol 35(10), 2898–2907. https://doi.org/10.1002/joc.4180

Yang, X., Xie, X., Liu, D.L., Ji, F., Wang, L., 2015. Spatial interpolation of daily rainfall data for local climate impact assessment over Greater Sydney Region. Adv Meteorol 2015. https://doi.org/10.1155/2015/563629

Zhang, J., Howard, K., Langston, C., Vasiloff, S., Kaney, B., Arthur, A., van Cooten, S., Kelleher, K., Kitzmiller, D., Ding, F., Seo, D.J., Wells, E., Dempsey, C., 2011. National mosaic and multi-sensor QPE (NMQ) system description, results, and future plans. Bull

Am Meteorol Soc 92(10), 1321–1338. https://doi.org/10.1175/2011BAMS-D-11-00047.1
Zhang, T., Li, B., Wang, J., Hu, M., Xu, L., 2016. Estimation of areal mean rainfall in remote areas using b-shade model. Adv Meteorol 2016. https://doi.org/10.1155/2016/7643753

Tables and Figures

Table 1. Properties of the weather station networks used in this study

Weather Network Inventory Specifications	ASOS	AWS	Composite Radar HSR
Number of stations	96	504	10
Start Date (Different for each site)	April/1904	July/1989	September/16/2019
Data type	Point	Point	Grid
Spatial Coverage	-	-	500 m (2305 × 2881)
Timescale	Minutely, hourly, daily, monthly, yearly	Minutely, hourly, daily, monthly, yearly	5 min
File format	CSV, XML	CSV, XML	Bin (binary), PNG
Download link	http://data.kma.go.kr		

Table 2. Hydrologic unit map information used in this study

Specifications \ Basin classification		Large Basin (LBSN)	Middle Basin (MBSN)	Standard Basin (SBSN)
Total number of units		20	106	808
Area (km^2)	Mean	5378.06	951.87	128.97
	Maximum	34428.1	2483.82	700.45
	Minimum	505.52	43.87	7.46
Download link		http://www.nsdi.go.kr		

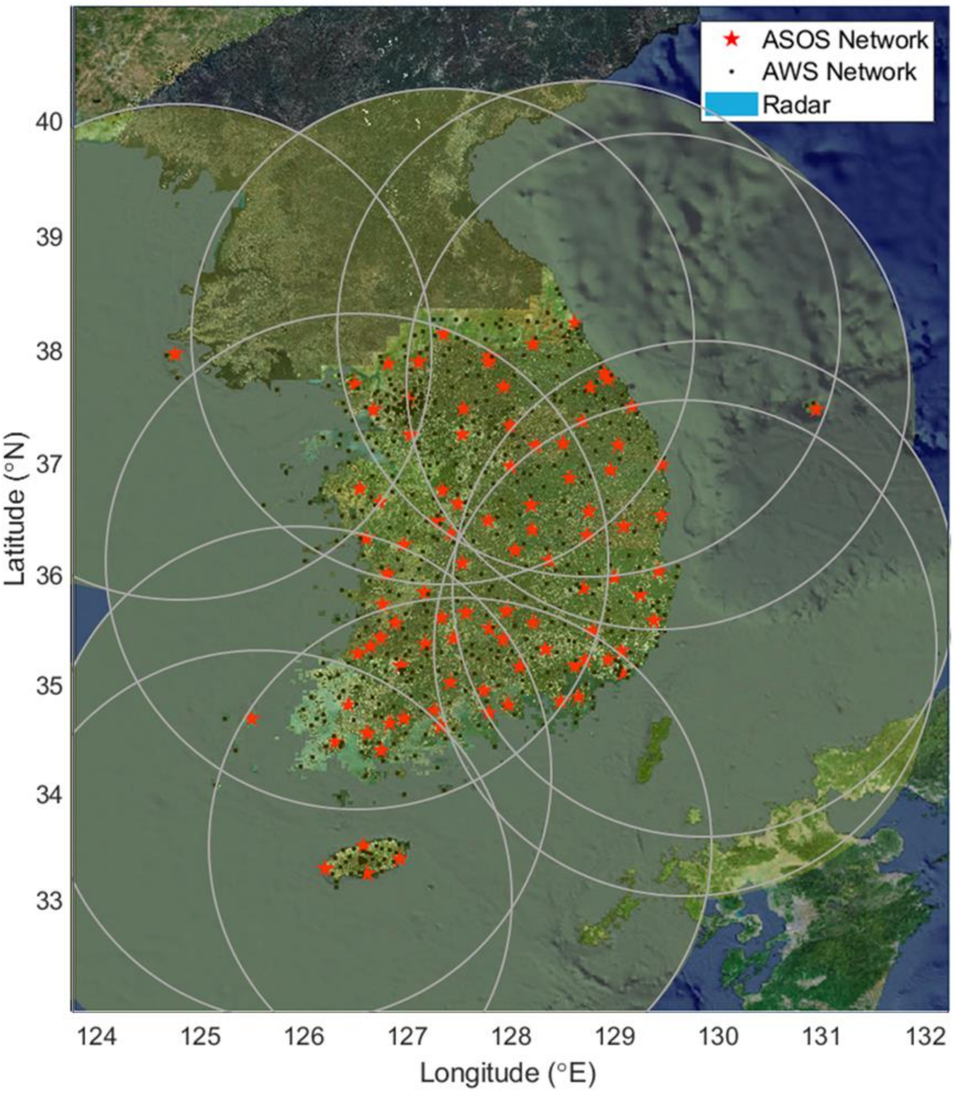

Figure 1. Map showing precipitation over a dense network along with weather radar system domain over South Korea

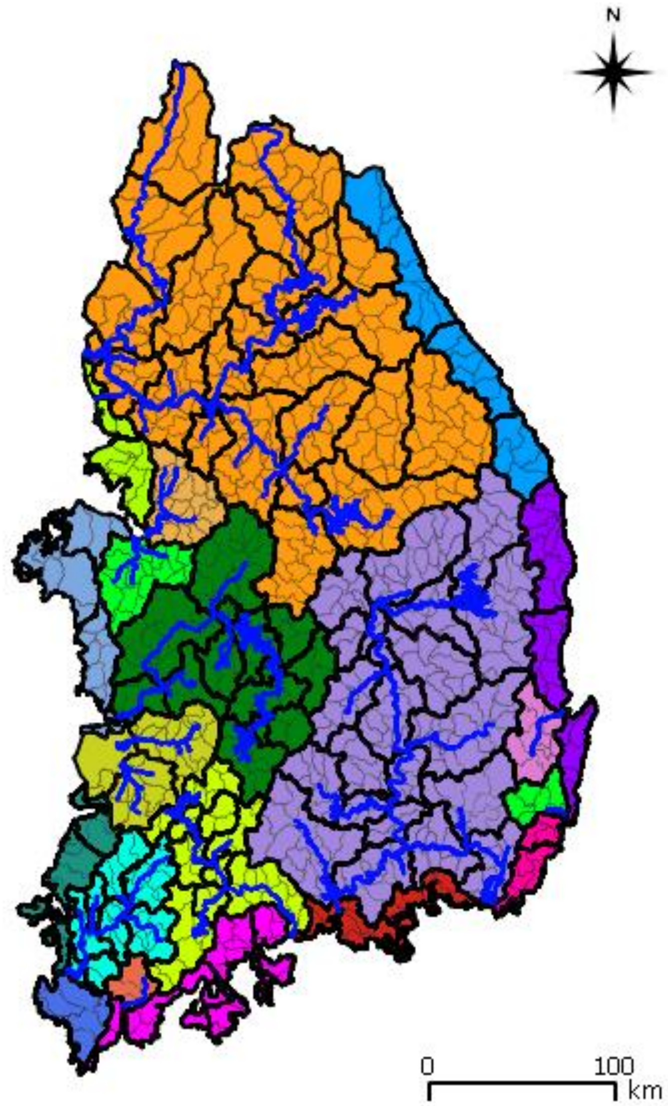

Figure 2. Map showing hydrologic units over South Korea, with different colors indicating the 20 large basins (LBSN). The boundaries of the 106 middle-size (MBSN) and 808 standard-size (SBSN) basins are marked by solid black and gray lines, respectively. The national rivers of South Korea are delineated by blue lines on the map

Step 1. Compare ASOS and AWS Measurements

- Identify Locations: Determine specific locations within a hydrologic unit for comparison.
- Collect Data: Gather rainfall measurement data from both ASOS and AWS.
- Analyze Differences: Compare the measurements in terms of amounts and spatial patterns

Step 2. Evaluate Radar Performance in Estimating Areal Rainfall

- Replace Observed Data with Radar Estimates: For the same locations, use radar-based rainfall estimates.
- Explore Station Network Density Impact: Analyze how the density of ASOS and AWS stations affects the estimation accuracy.
- Initial Comparison with True Areal Rainfalls: Compare these radar estimates to actual observed areal rainfalls for a consistent comparison.

Step 3. Compare Two Types of Radar-Derived Areal Rainfall Data

- Pointwise Radar Estimates: Focus on radar estimates that correspond to specific locations of the weather stations.
- Gridded Radar Estimates: Look at radar rainfall estimates that are averaged over the entire basin.
- Perform Comparison: Assess the differences between these two approaches to understand how data aggregation affects rainfall estimation.

Figure 3. Detailed three-step modeling process for areal rainfall estimation: analyzing the impact of weather station network density and watershed area on basin-scale hydrological analysis

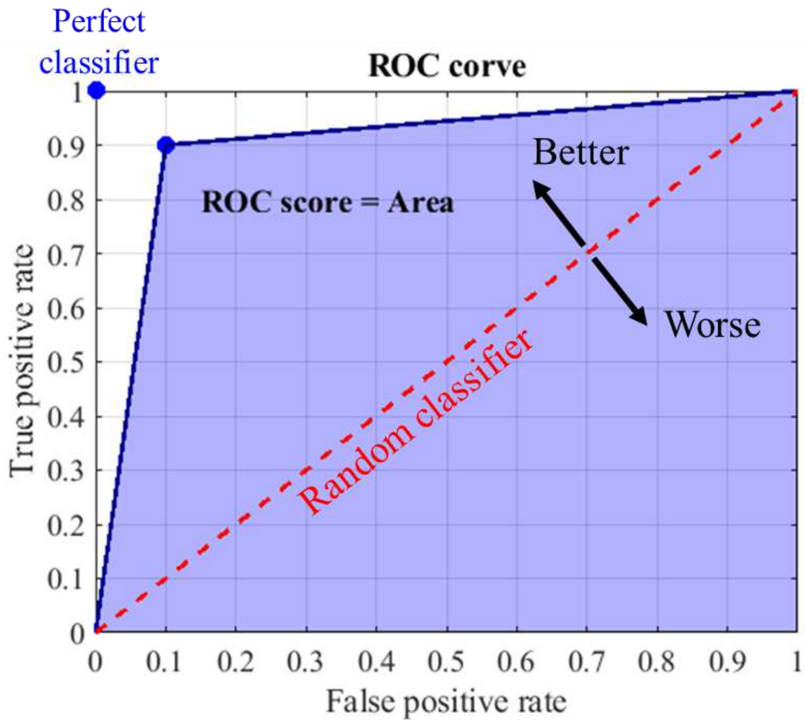

Figure 4. ROC space for "better" and "worse" classifiers. The space above the diagonal (dotted red line) represents similar patterns between areal rainfall occurrence sequences (better space); the space below the line represents different patterns between areal rainfall occurrences over time (worse space). The point at (0, 1) represents an identical sequence between the two areal rainfall occurrences over time and vice versa in the space around (1, 0)

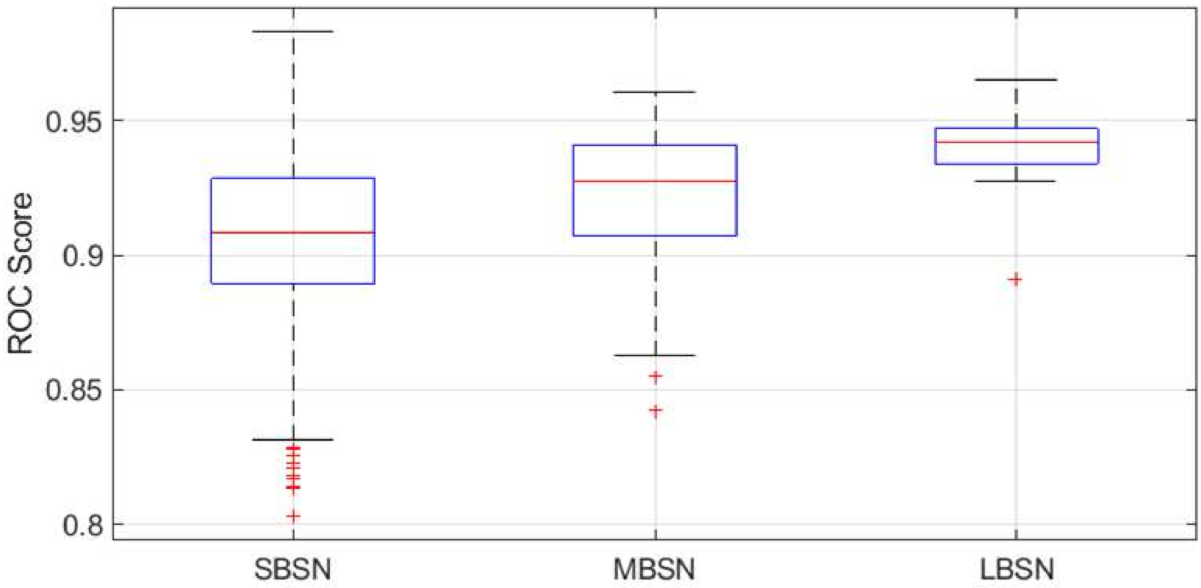

Figure 5. Distribution of ROC scores for the three types of hydrologic units classified according to the basin scale. The ROC score represents similarities of the two areal rainfalls estimated by the ASOS and AWS networks. (SBSN: standard basin, MBSN: middle basin, and LBSN: large basin)

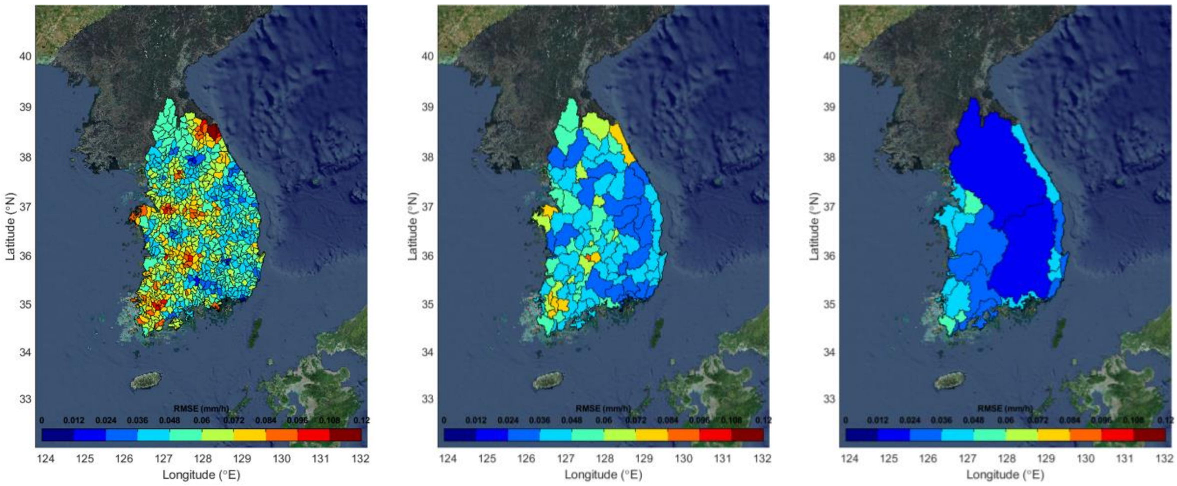

a) SBSN b) MBSN c) LBSN

Figure 6. Spatial distribution of RMSE between the areal rainfalls constructed using the TW method on the ASOS and AWS networks for the three basin sizes. The comparisons were made with complete rainfall sequences, including zero rainfall. (SBSN: standard basin, MBSN: middle basin, and LBSN: large basin)

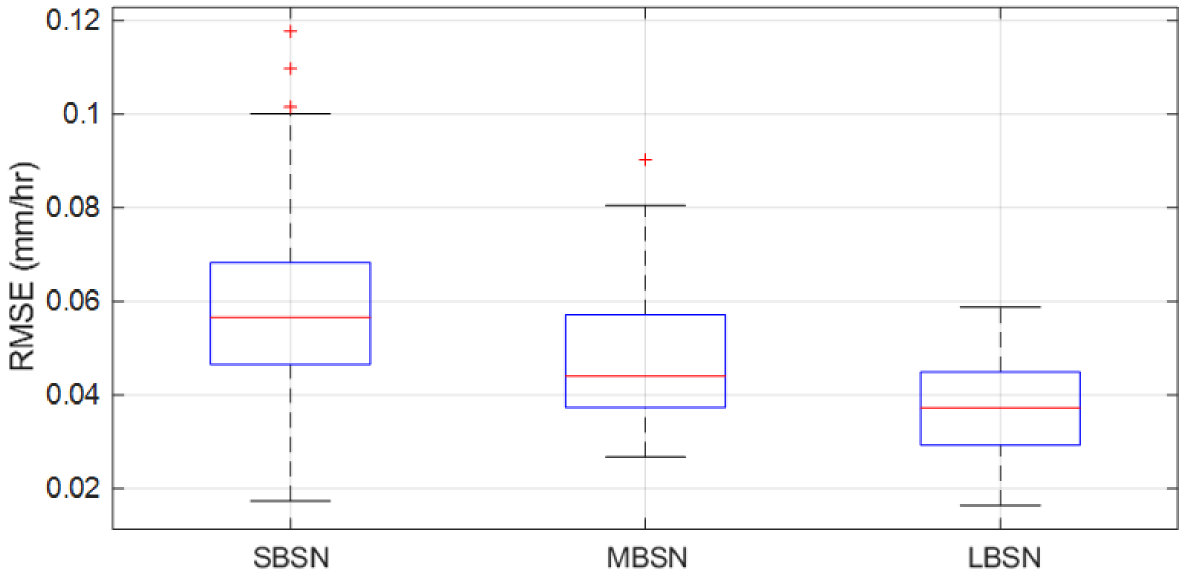

Figure 7. Boxplot showing RMSE distribution between the areal rainfalls constructed using the TW method on the ASOS and AWS networks over the three basin sizes. The comparisons were made with the complete rainfall sequences, including zero rainfall. (SBSN: standard basin, MBSN: middle basin, and LBSN: large basin)

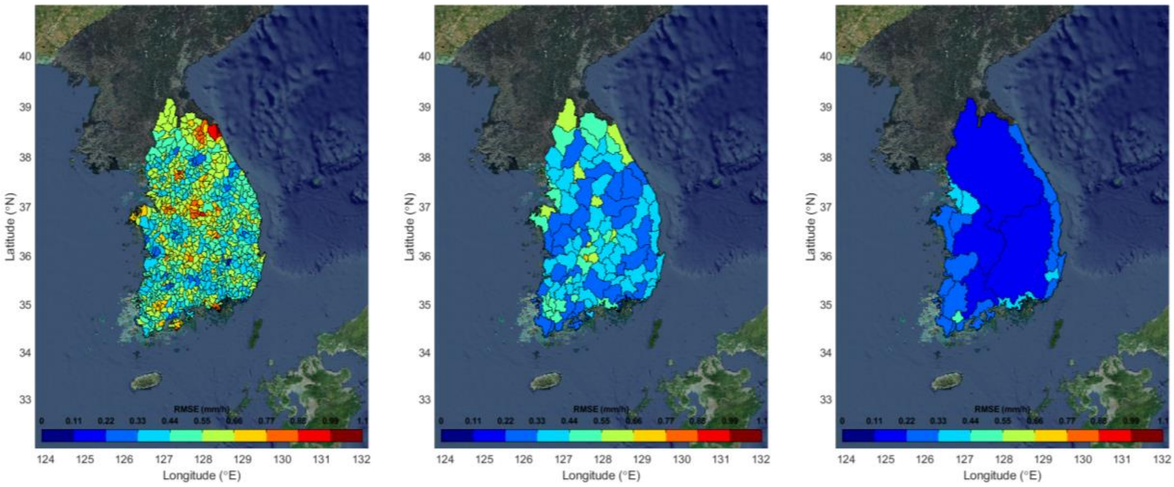

a) SBSN b) MBSN c) LBSN

Figure 8. Spatial distribution of RMSE between the areal rainfalls constructed using the TW method on the ASOS and AWS networks for the three basin sizes. The comparisons were made with the rainfall sequences, excluding zero rainfall. (SBSN: standard basin, MBSN: middle basin, and LBSN: large basin)

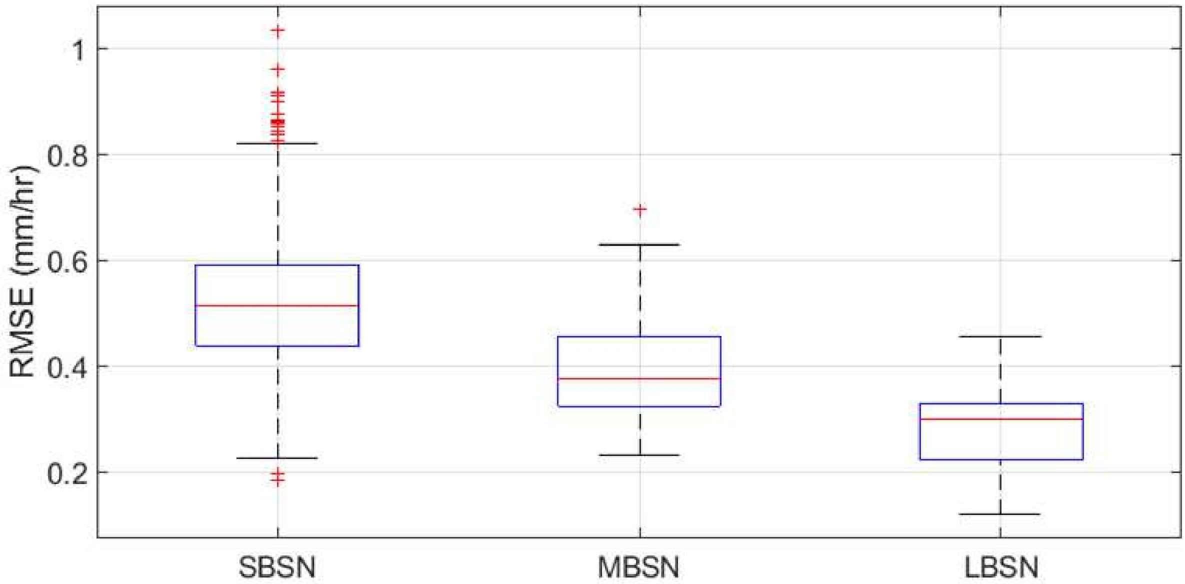

Figure 9. Boxplot of RMSE distribution between the areal rainfalls constructed using the TW method on the ASOS and AWS networks over the three basin scales. The comparison was made with the rainfall sequences excluding zero rainfall. (SBSN: standard basin, MBSN: middle basin, and LBSN: large basin)

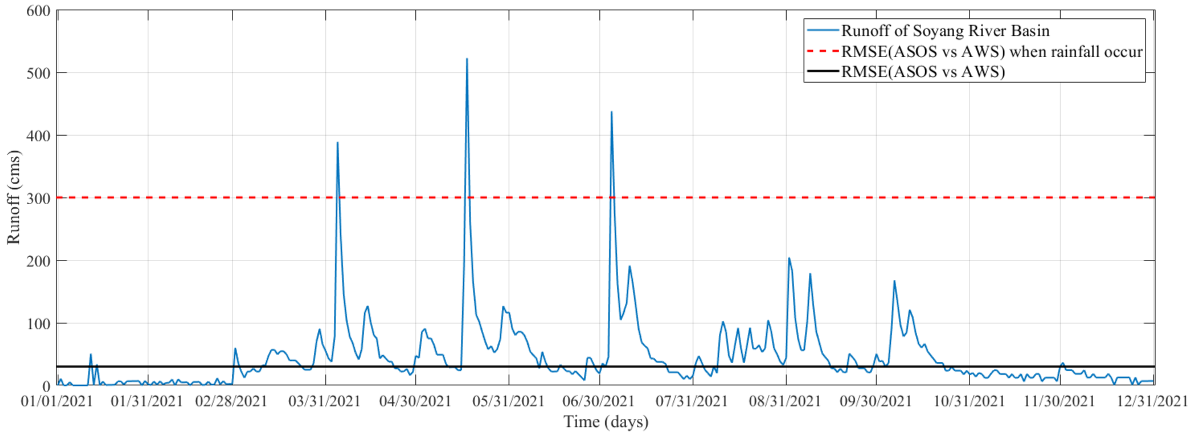

Figure 10. Observed runoff series of the Soyang River basin from January 1st, 2021, to December 31st, 2021. The black-solid and red dashed lines are the average RMSE in m^3/s, including and excluding zero rainfalls, respectively

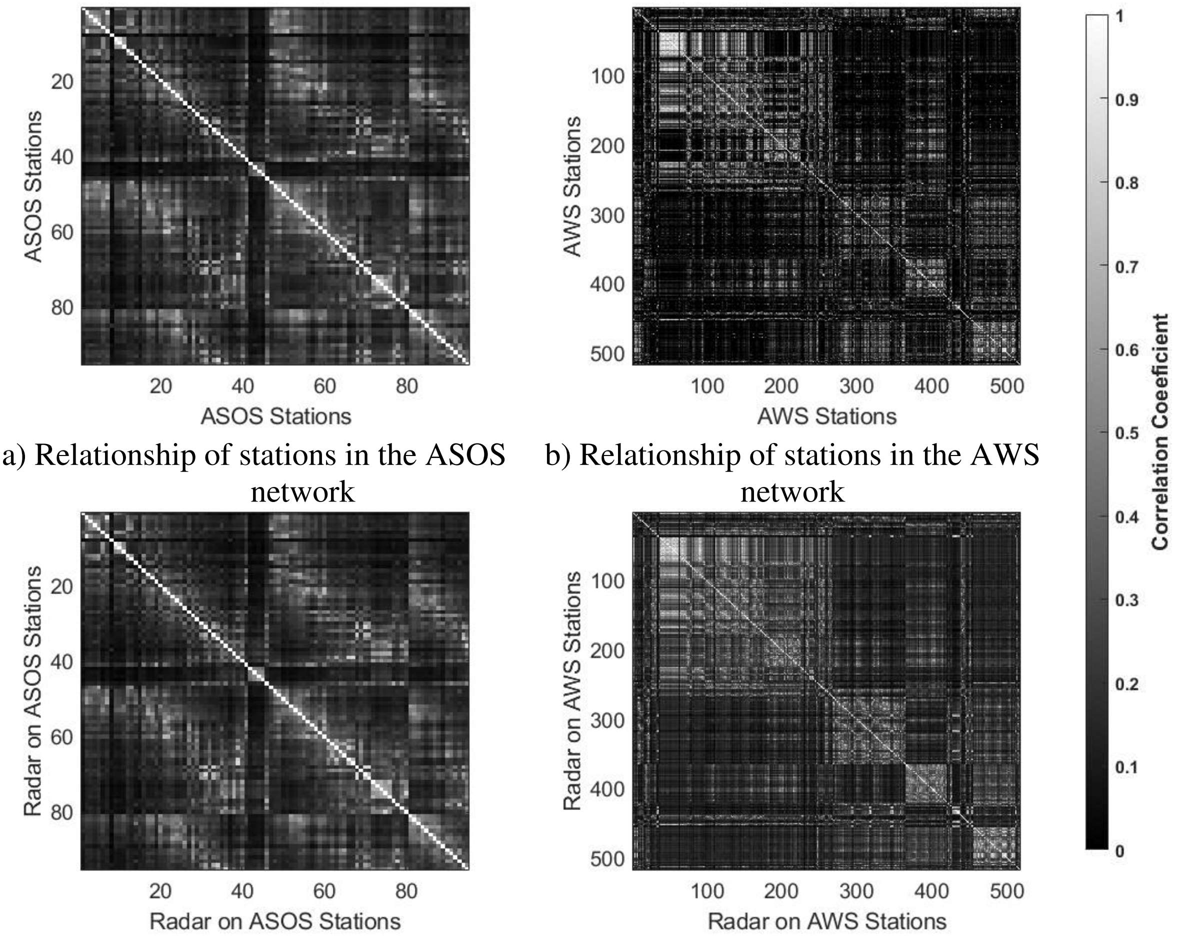

a) Relationship of stations in the ASOS network

b) Relationship of stations in the AWS network

c) Relationship of radars located in the ASOS network

d) Relationship of radars located in the AWS network

Figure 11. Spatial dependency across weather stations with correlation coefficients: a) ASOS network, b) AWS network, c) radar rainfall estimates on the ASOS network, d) radar rainfall estimates on the AWS network. Initially, radar-based rainfall data for the locations of 96 ASOS and 504 AWS stations are extracted. The TW method is then utilized to construct areal rainfall measurements. Subsequently, cross-correlations of the precipitation series across both ASOS and AWS stations are calculated to assess the spatial dependency among weather stations

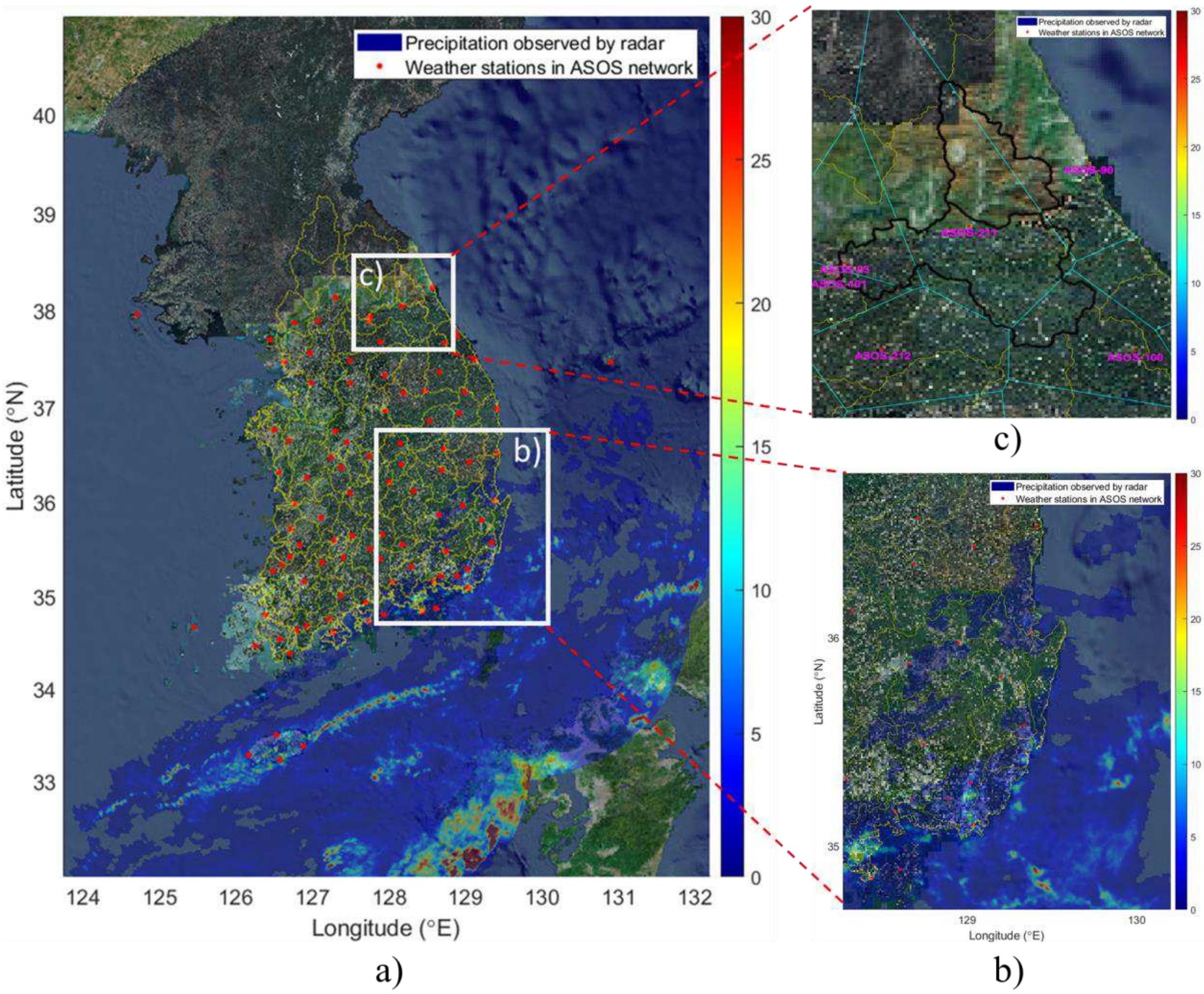

Figure 12. Radar image at 2022-04-26 13:10 – 13:15 (a). The red dots are weather stations in the ASOS network. The area defined by the yellow line is a middle-size basin (MBSN). Figure (b) is an enlarged area covered by rainfall fields, and figure (c) shows the Thiessen polygon map for the Soyang River basin with the ASOS station codes

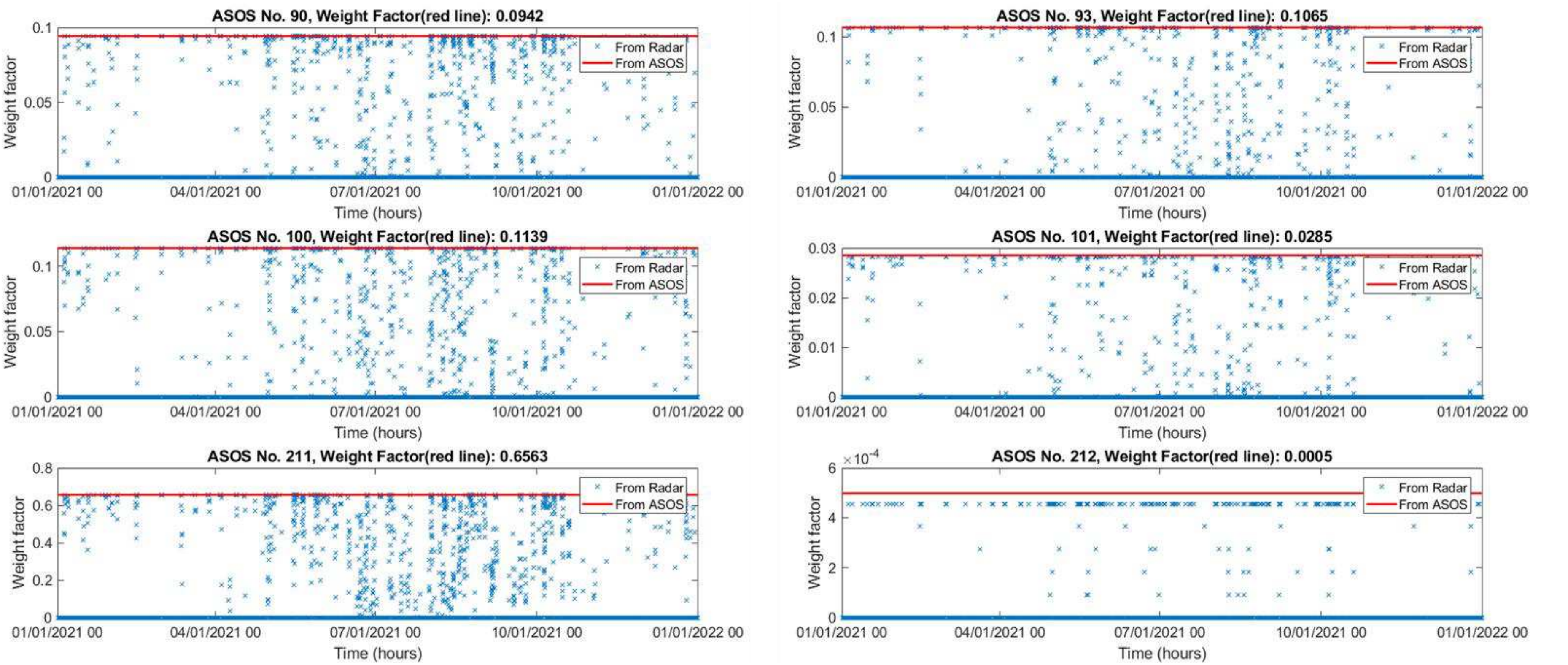

Figure 13. Weighting factor sequences from 01:00 on January 1st, 2021, to 24:00 on December 31st, 2021, for six contributing areas with the representative gauging stations in the Soyang River basin. Factors are obtained by repeatedly estimating areas covered by actual rainfall fields from radar rainfall networks over time with respect to the Thiessen polygons in the Soyang River basin. The red solid line represents the existing TW weighting factor

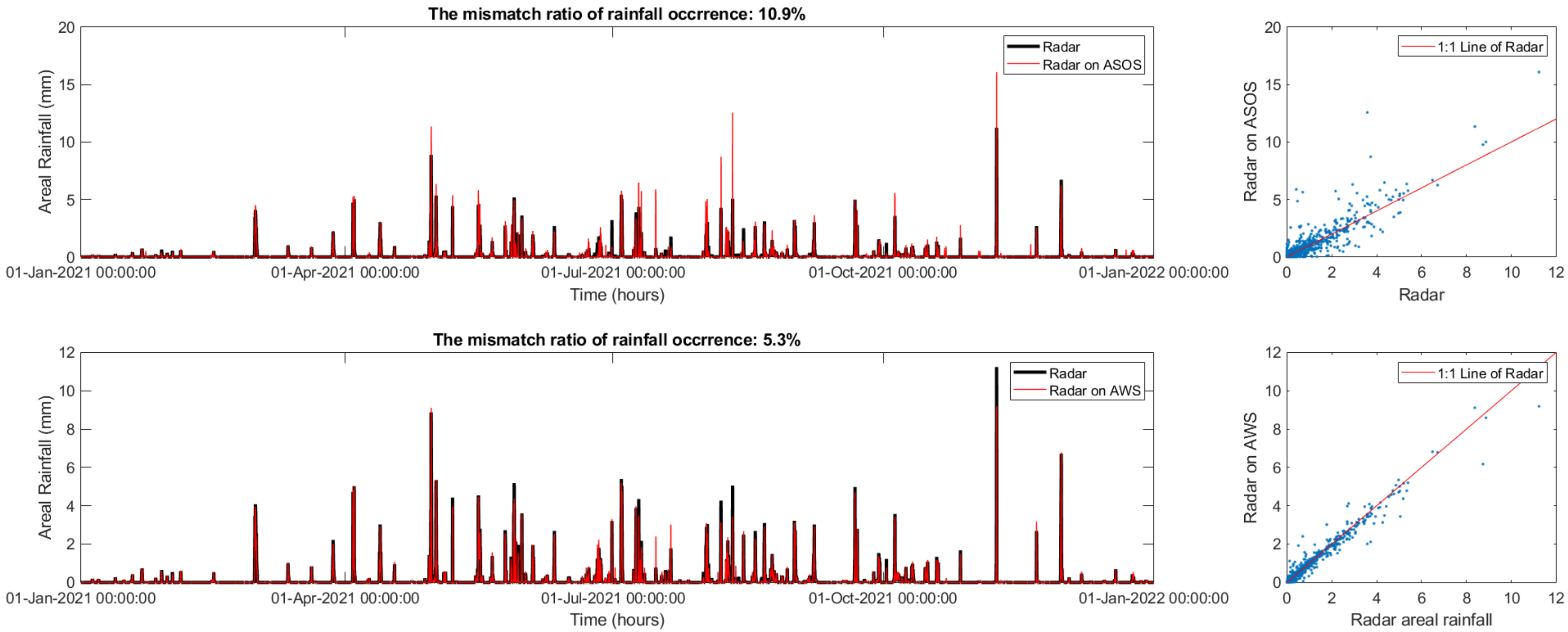

Figure 14. Areal rainfall time series and scatter plot from 01:00 on January 1st, 2021, to 24:00 on December 31st, 2021. The weighing factors informed by the ASOS (top panel) and AWS (lower panel) networks are used to construct the areal rainfall series for comparison with the areal rainfalls averaged over gridded radar rainfalls covering the Soyang River basin

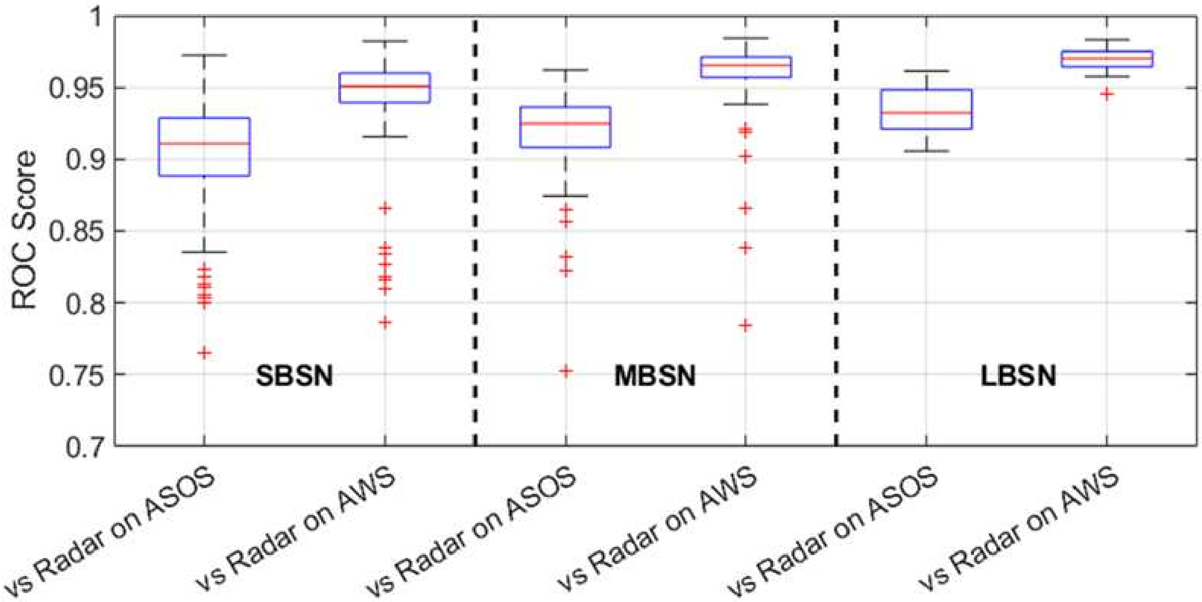

Figure 15. Boxplots of ROC scores for basin-scale type. Here, the ROC score was obtained by comparing two areal rainfalls: averaged gridded radar rainfalls over the hydrologic unit and radar-based areal rainfalls on the ASOS and AWS networks. (SBSN: standard basin, MBSN: middle basin, and LBSN: large basin)

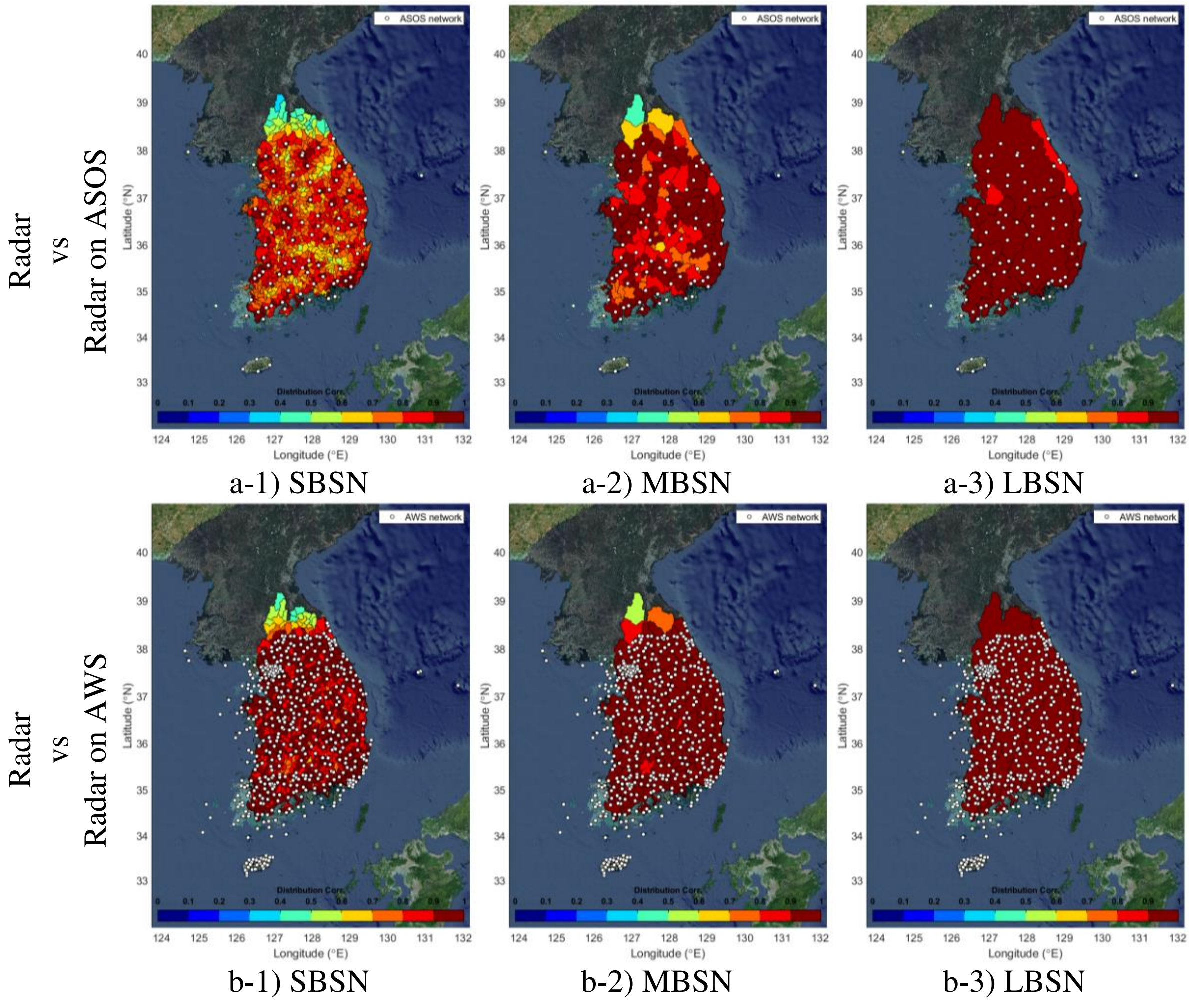

Figure 16. Correlation coefficient distribution between the radar-based areal rainfalls constructed using the TW method on the ASOS and AWS networks and true areal rainfalls for the three basin sizes. The transition from SBSN (left) to LBSN (right) shows the case with increasing basin scale, while the transition from Radar on ASOS (top) to Radar on AWS (bottom) represents the increasing density of the weather station network. (SBSN: standard basin, MBSN: middle basin, and LBSN: large basin)

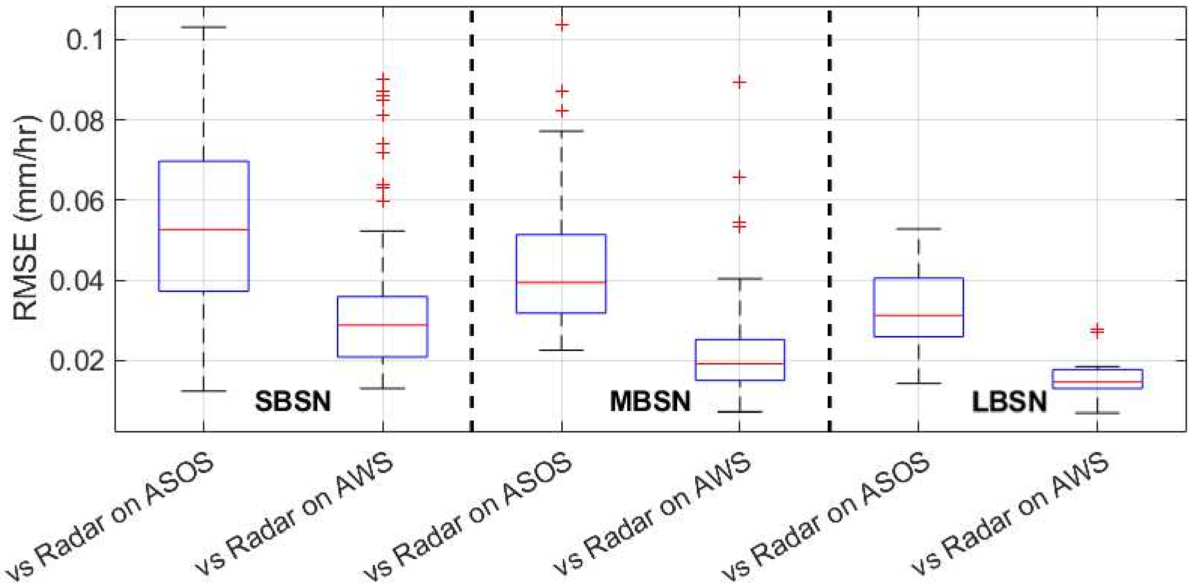

Figure 17. Boxplot of the RMSE distribution between the areal rainfalls constructed using the TW method on the ASOS (or AWS) networks and true areal rainfalls over the three basin sizes. The comparisons were made with the complete rainfall sequences, including zero rainfall. (SBSN: standard basin, MBSN: middle basin, and LBSN: large basin)

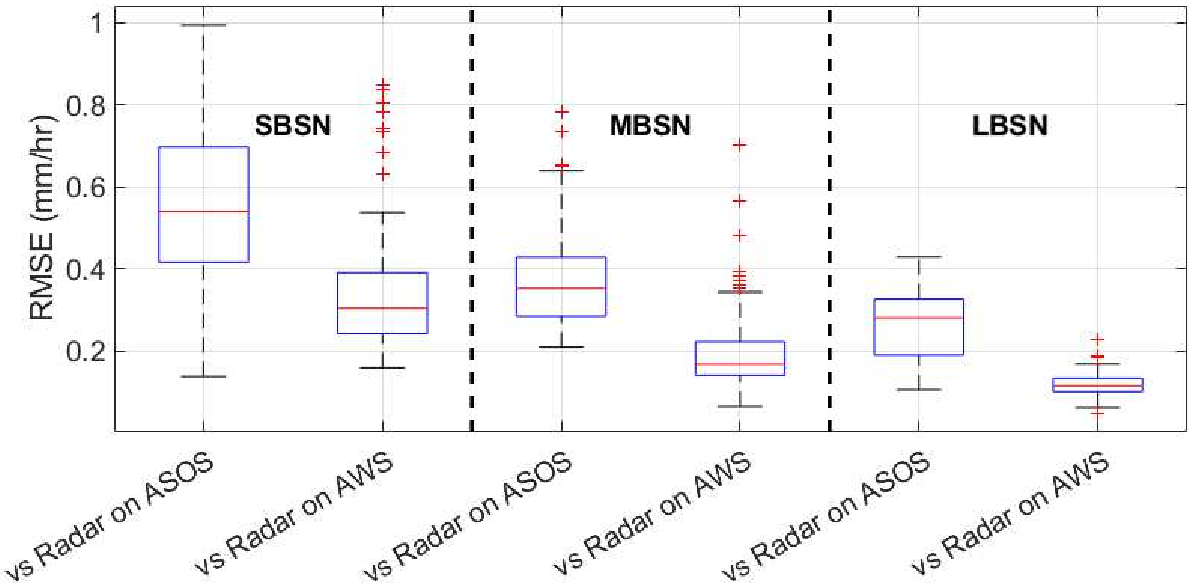

Figure 18. Boxplot of the RMSE distribution between the areal rainfalls constructed using the TW method on the ASOS (or AWS) networks and true areal rainfalls over the three basin sizes. The comparisons were made with the complete rainfall sequences, excluding zero rainfall. (SBSN: standard basin, MBSN: middle basin, and LBSN: large basin)

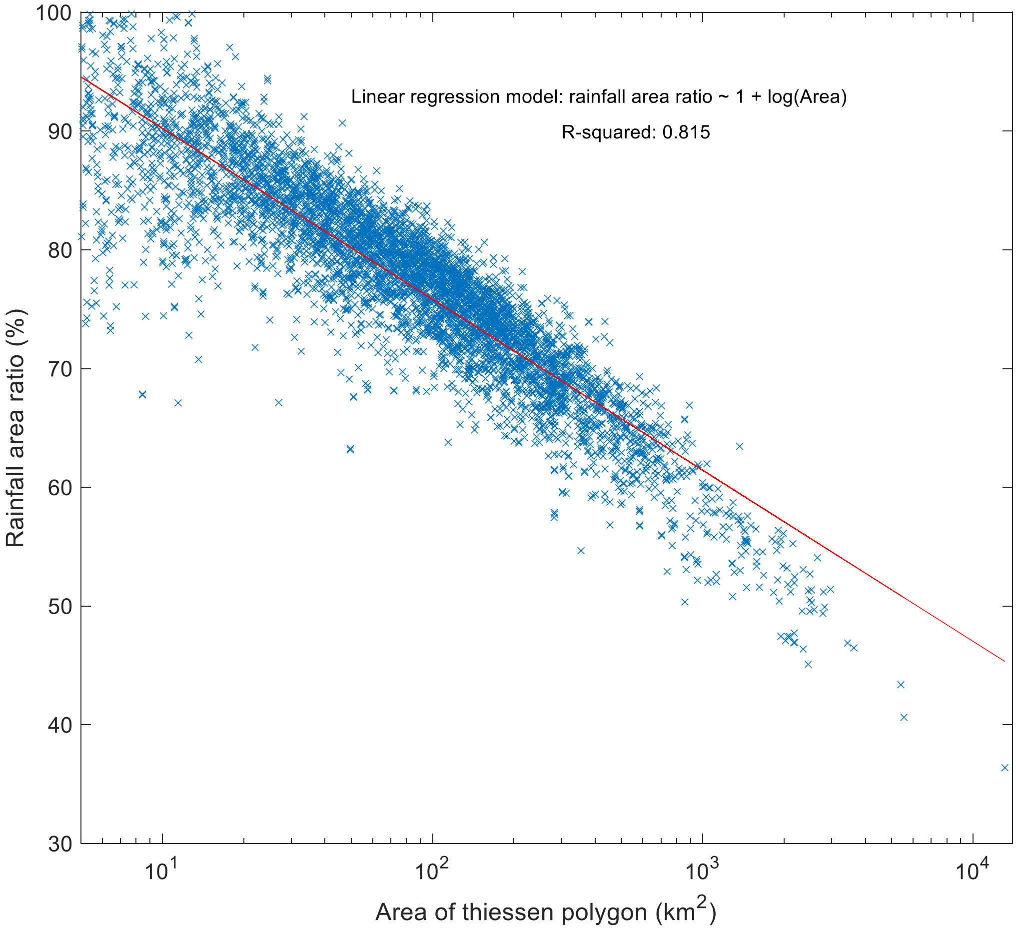

Figure 19. Contributing area ratio on the Thissen polygon area for all basins over South Korea in 2021 and all rainfall time series. The red solid line is the result of a linear regression model